PAPER • OPEN ACCESS

Fracture mechanics of additive manufactured crack-like notches by digital image correlation

To cite this article: Giangiacomo Minak and Nenad Drvar 2022 *IOP Conf. Ser.: Mater. Sci. Eng.* **1214** 012003

View the article online for updates and enhancements.

Fracture mechanics of additive manufactured crack-like notches by digital image correlation

Giangiacomo Minak[1], Nenad Drvar[2]

[1]Alma Mater Studiorum – Università di Bologna, via Fontanelle 40, 47131 Forlì, Italy
[2]Topomatika d.o.o. Industrijska ulica 3, Novaki HR-10431, Sveta Nedelja, Croatia

giangiacomo.minak@unibo.it

Abstract. The rapid development of a variety of Additive Manufacturing (AM) techniques is witnessed by the large interest of the scientific community. Among the numerous new features offered by these techniques, very lately the possibility of including cracks of any shape, direction, and position inside AM samples to validate FEM models was explored. Therefore, the necessity arose of full-field measurement techniques that would allow the evaluation of the fracture mechanics parameters in the cases of both linear elastic and partially plastic materials, as a function of the fracture modes. Invented in the '80 of the XX century, the Digital Image Correlation (DIC) in recent years has taken place in nearly every laboratory. It is used to measure displacements, and by numerical differentiation or coupling with Finite Element Method, to calculate strains at different spatial scales. In particular, two procedures that were successfully employed on a specific kind of specimens, based on DIC at a small scale near the crack-tip, in this paper are shown in detail.

1. Introduction

Additive manufacturing in the last few years demonstrated unique capabilities and attracted much research interest. Industrial applications, which include automotive, aerospace, biomechanics, take advantage of the possibility of tailoring the characteristics of the products utilizing shapes not attainable using the classical subtractive manufacturing techniques.

The increasing use of AM components led to the study of the fracture mechanics of the relevant base materials, as a function of the process parameters and the built direction. An extensive analysis on the topic is reported in a recent review by Khosravani et al [1].

A new application for these techniques, proposed by Brugo et al. [2], consists in the embedding of a crack of any shape and position in AM components. In this way, the validation possibilities for numerical models can be greatly widened at least in terms of global stiffness and resistance. However, full-field measurement methods are needed to evaluate the local stress and strain at the crack-tip and to follow its evolution.

The use of the Digital Image Correlation technique to study fracture mechanics problems was introduced in the mid '80 [3,4], few years after the invention of the method in 1982 by Peters, Sutton et al. [5-6] and in the past few years emerged over other methods like the Object Grating [7].
In this paper, two procedures based on the (DIC) to evaluate the fracture behavior of AM components with embedded cracks are described.

Nowadays, the DIC is a relatively cheap, easy, and widely available optical technique used to measure the full displacement and strain field. It requires just one or two cameras, for 2D and 3D measurements respectively, of sufficiently high resolution and an algorithm to correlate the images. The correlation is performed by exploiting a speckle pattern (obtained by spray paint or ink powder) on the surface of the sample. This random pattern is a key point for the correlation algorithm, which matches subsets of pixels in consecutive images. By locating a point in the undeformed and the deformed image the displacement can be calculated.

While the displacement field is computed directly by DIC, the strain field is calculated by numerical differentiation of the displacement, with an inevitable introduction of noise. This is the reason why fitting methods usually are applied to the displacement field rather than to the strain one.

These displacement fields can be used to quantitatively characterize the fracture behavior of the material, and in particular, they can be exploited to estimate the stress intensity factors (SIFs).

Generally speaking, for linear elastic materials two main approaches to the fitting of theoretical models on the full displacement fields are shown in the literature. The first one is based on guessing a general form of an analytical function and fitting this to the displacement experimental data [8-10]. The second approach, which is applied in this paper, is based on the Williams' model [11-13], and the fitting on the experimental data is done by considering the first n term of the Williams expansion of the displacement.

The stress intensity factors (SIFs) are suitable parameters only in the case of a material that can be considered linear elastic. On the other hand, if the material exhibits an elastic-plastic behavior, the J-integral, originally proposed by Rice [14], can be successfully used to characterize the fracture mechanics behavior.

The J-integral represents the strain energy release rate or energy per unit fracture surface area of a material, and it is usually calculated from the integration of the experimental load-displacement curve.

However, this technique is suitable only for laboratory tests, in which the geometry factors for the specific specimen are known, and the load-displacement curve can be measured.

On the contrary, on a complex structure under various loads, it is generally impossible to compute the geometrical factors and the load-displacement boundary conditions for the specific position in which the crack is located.

To fit the purpose of analyzing cracks in a generic position of a real component, an alternative method consists of computing the J-integral from the displacement fields around the crack tip, measured by DIC. The DIC-based technique computes numerically the J-integral along a rectangular contour of the DIC grid [15-19].

To perform the J-integral calculation, displacement, strain, and stress fields must be known. The displacement and strain field are obtained from the DIC, while the stress-strain constitutive relation of the material must have been previously determined (e.g. by means of the Ramberg-Osgood model, as it is done in [20]).

In this paper the application of the two DIC based methods is shown in the case of two different materials, one Martensitic steel which can be considered linear elastic [21] and a Polyamide [22] which exhibits marked plasticity.

The experiments were performed on IASCB specimens [23-25] manufactured by Selective Laser Sintering (SLS). During the AM process, crack-like notches with different angles were embedded in the specimen and different values of support spans were considered in the test. Three repetitions were done for each specimen type and test condition.

The comparison with the results obtained employing standard methods for different fracture mode I-II mixity is shown.

2. Materials and Methods

2.1. Materials

The metallic specimens were manufactured by the EOSINT M 280 SLS machine (EOS GmbH), using the EOS Maraging Steel MS1 steel powder, with a chemical composition corresponding to the European 1.2709 classification. Other manufacturing details and material properties can be found in [21].

The polymeric specimens were produced by an EOS Formiga P100 SLS machine (EOS GmbH), using fine polyamide PA 2200 powder purchased from Prototal Plastic Design and Service (Götene, Sweden). The laser-sintered specimens were manufactured from mixed powder, recycled and new in equal proportions [22].

During the fabrication via the SLS technology, the specimens were oriented with the thickness in the built direction for both kinds of specimens.

2.2. IASCB Specimens

The IASCB specimen is a semicircular disk with an embedded radial edge-crack, tilted with respect to the load direction. The fracture test consists of the application of a vertical force, with the specimen located on two bottom supports, as shown in Figure 1. By varying the support spans and the crack tilt, it is possible to obtain a large variety of mixed I/II modes. In the cases under study, the thickness was 6 mm, the disk radius 60 mm and the crack length 24 mm. One of the spans was kept fixed at 42 mm and the other was varied, together with the crack angle, to change the mode mixity defined as $M = 2/\pi \, \mathrm{atan}(K_{II}/K_I)$ where K_I and K_{II} are the Sifs in mode I and II respectively.
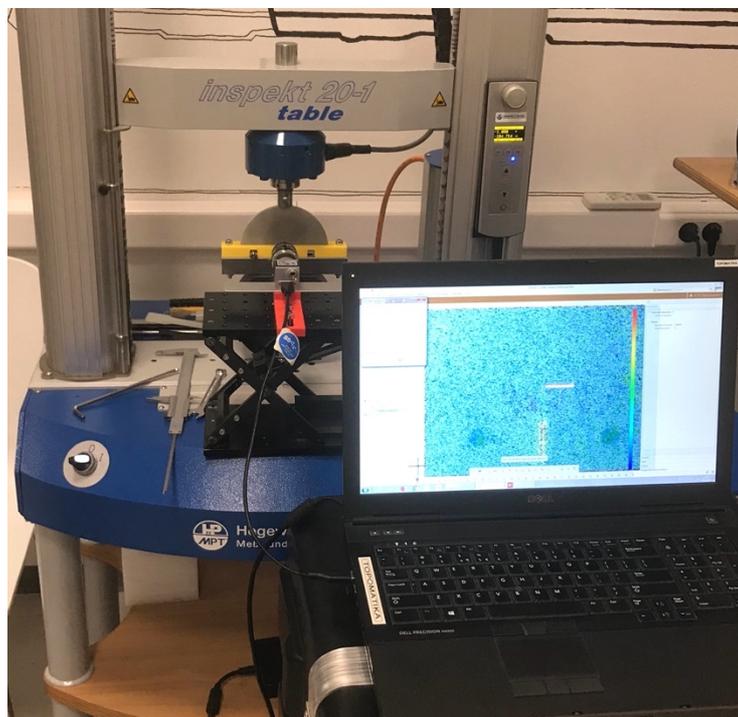

Figure 1: Experimental Setup

2.3. Digital Image Correlation

The 2D DIC system used to evaluate the full displacement field around the crack tip (in a window of 12 mm × 9 mm) consisted of a 10 MP Basler ace acA3800-14uc camera (Basler, Ahrensburg, Germany)

equipped with Basler lens C125-2522–5 M-P f25 mm (Basler, Ahrensburg, Germany) and a custom led lamp.

A 2D measurement setup instead of 3D was chosen for a combination of measurement system reasons, specimen shape and loading conditions and postprocessing methodology. Since it is possible to assume that there are no large displacements that would cause the specimen to move significantly in the field of view, any errors that are the outcome of lens imperfections can be neglected considering that displacements are pretty much localized. When measuring small field of view (FOV) 2D setup gives more flexibility with FOV sizes, since the number of pixels in the camera is constant but just by changing the lens settings and distance from the object it is possible to adjust the 2D FOV practically to any desired size, compared to 3D DIC setups which tend to have the FOV predefined by the size of the available calibration objects. Care must be taken with 2D setups since the camera chip needs to be perfectly parallel to the specimen surface, and the specimen should have negligible out of plane displacement and rotations during the test since there is no possibility to compensate for out of plane rigid body motion, which is possible with 3D setups. Moreover, in 3D setups, the surface must be smooth enough not to cause problems to DIC when viewed from different sides (this should be considered for big magnifications and if 3D printed specimens with large layers or methods with visible layers are used).

The images were acquired by exploiting the GOM Snap 2D free software and processed by GOM Correlate (GOM GmbH, Braunschweig, Germany). GOM Snap can use USB cameras compatible with GenICam protocol, but as in the case of the present paper the loading application must be slow enough not to cause additional errors if using cameras with rolling shutters.

A black speckle pattern was spray-painted on the specimens (which naturally exhibits a white surface), as required by the digital correlation algorithm.

The DIC parameters were set according to the study of Palanca et al. [26], as follows: 19 pixels facet size, 16 pixels point distance, 8 facets spatial filter (median) and 3 time-step temporary filters (median). This parameter combination allows obtaining an optimal compromise between the spatial resolution and the precision of the displacement field measurement around the crack tip.

2.4. Evaluation of stress intensity factors by the DIC full displacement field

To model the displacement near the crack tip, the Williams' asymptotic formulation [27] was exploited. The u and v are the displacement along the crack axis (x-axis) and along an axis perpendicular to the former and contained in the crack plane (y-axis). Figure 2 shows the reference system used, with the origin located into the crack tip.
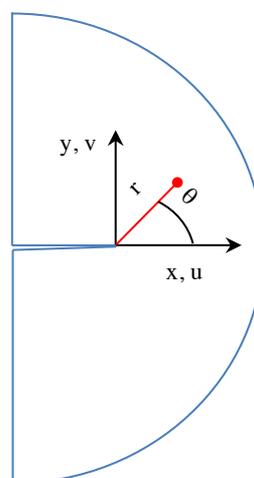

Figure 2: Reference system

In mode I, u and v are expressed as functions of the polar coordinates (r, θ), according to the series shown in Equations 1-2.

$$u_I = \sum_{n=1}^{\infty} \frac{r^{\frac{n}{2}}}{2\mu} a_n \left\{ \left[\kappa + \frac{n}{2} + (-1)^n \right] cos \frac{n\theta}{2} - \frac{n}{2} cos \frac{(n-4)\theta}{2} \right\} \tag{1}$$

$$v_I = \sum_{n=1}^{\infty} \frac{r^{\frac{n}{2}}}{2\mu} a_n \left\{ \left[\kappa - \frac{n}{2} - (-1)^n \right] sin \frac{n\theta}{2} + \frac{n}{2} sin \frac{(n-4)\theta}{2} \right\} \tag{2}$$

In mode II, u and v are computed as functions of the polar coordinates (r, θ), according to the series shown in Equations 3-4.

$$u_{II} = -\sum_{n=1}^{\infty} \frac{r^{\frac{n}{2}}}{2\mu} b_n \left\{ \left[\kappa + \frac{n}{2} - (-1)^n \right] sin \frac{n\theta}{2} - \frac{n}{2} cos \frac{(n-4)\theta}{2} \right\} \tag{3}$$

$$v_{II} = \sum_{n=1}^{\infty} \frac{r^{\frac{n}{2}}}{2\mu} b_n \left\{ \left[\kappa - \frac{n}{2} + (-1)^n \right] cos \frac{n\theta}{2} + \frac{n}{2} cos \frac{(n-4)\theta}{2} \right\} \tag{4}$$

where $\mu = E/(2+2\nu)$ is the shear modulus and $\varkappa = (3-\nu)/(1+\nu)$ for plane stress and $\varkappa = 3-4\nu$ for plane strain condition, respectively being E the elastic modulus and ν the Poisson ratio; a_n and b_n are the model parameters. The specimens are considered subjected to plane stress condition [28].

For mixed modes, the displacement fields can be obtained by the superimposition of the displacement of pure mode I and pure mode II, as shown in Equations 5-6

$$u = u_I + u_{II} \tag{5}$$

$$v = v_I + v_{II} \tag{6}$$

The values of K_I and K_{II} are calculated from the value of the Williams model parameters as shown in Equations 7-8.

$$K_I = a_1 \sqrt{2\pi} \tag{7}$$

$$K_{II} = -b_1 \sqrt{2\pi} \tag{8}$$

Four additional parameters (three translations and the rotation around the z-axis, perpendicular to the crack plane) were accounted to compensate rigid motions while performing the fitting, as done also in [28] and [29]. This approach is suitable when the material exhibits small-scale plastic deformation, on the other hand, it introduces non-linearity in the fitting parameters because the polar coordinates (r, θ) are modified as shown in Equations 9-10.

$$r = \sqrt{(x - x_0)^2 + (y - y_0)^2} \tag{9}$$

$$\theta = arctg\left(\frac{y - y_0}{x - x_0}\right) \tag{10}$$

2.5. J-integral computation by means of DIC

As said, the J-integral represents the strain energy release rate or energy per unit fracture surface area of a material. It is mathematically defined as a line-integral, as shown in Equation 11:

$$J = \int_{\Gamma} \left(W dy - t_i \frac{\partial u_i}{\partial x} ds \right) \tag{11}$$

where Γ is the integration path, W is the strain energy density, $t = \sigma \hat{n}$ is the surface traction vector ($\hat{n}$ is normal to the curve Γ and σ is the Cauchy stress tensor). The most important property of the J-Integral is that it does not depend on the path used for the integration. In our case, since the DIC data are defined on a rectangular discrete grid the definition of the J integral has to be suitably adapted. If the grid is sufficiently dense this is an acceptable approximation [16, 30, 31]. The integration is carried out by using the trapezoidal rule. The integrand function *f* in the discrete domain can be rewritten as shown in Equation 12, being Δl the path increment:

$$f \Delta l = W \Delta y - t_i \frac{\Delta u_i}{\Delta x} \Delta s \tag{12}$$

Expanding the term of the traction vector in the hypothesis of plane stress, and summing on the index i leads to Equation 13:

$$f \Delta l = W \Delta y - \left[\frac{\Delta u_x}{\Delta x} \left(n_x \sigma_x + n_y \tau_{xy} \right) + \frac{\Delta u_y}{\Delta x} \left(n_y \sigma_y + n_x \tau_{xy} \right) \right] \Delta s \tag{13}$$

The rectangular path is divided in five parts, as shown in figure 3, so that each part can be further simplified as in Equations 14-17.
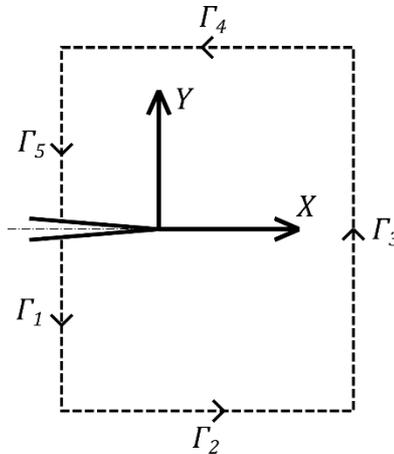

Figure 3: Rectangular path around the crack tip.

Path $\Gamma 1$ and Path $\Gamma 5$: $\hat{n} = (-1, 0)$, $\Delta s = -|\Delta gy|$, $\Delta y = -|\Delta gy|$ where $|\Delta gy|$ is the distance (constant and ≥ 0) between 2 points of the DIC grid along the y direction.

$$f \Delta l = \left(-W - \frac{\Delta u_x}{\Delta x} \sigma_x - \frac{\Delta u_y}{\Delta x} \tau_{xy} \right) |\Delta gy| \tag{14}$$

Path $\Gamma 2$: $\hat{n} = (0, -1)$, $\Delta s = |\Delta gx|$, $\Delta y = 0$ where $|\Delta gx|$ is the distance (constant and ≥ 0) between two points of the DIC grid along the x direction.

$$f \Delta l = \left(\frac{\Delta u_x}{\Delta x} \tau_{xy} + \frac{\Delta u_y}{\Delta x} \sigma_y \right) |\Delta gx| \tag{15}$$

Path $\Gamma 3$: $\hat{n} = (+1, 0)$, $\Delta s = |\Delta gy|$, $\Delta y = |\Delta gy|$

$$f\Delta l = \left(+W - \frac{\Delta u_x}{\Delta x}\sigma_x - \frac{\Delta u_y}{\Delta x}\tau_{xy}\right)|\Delta gy| \tag{16}$$

Path $\Gamma 4$: $\hat{n} = (0,+1)$, $\Delta s = -|\Delta gx|$, $\Delta y = 0$

$$f\Delta l = \left(\frac{\Delta u_x}{\Delta x}\tau_{xy} + \frac{\Delta u_y}{\Delta x}\sigma_y\right)|\Delta gx| \tag{17}$$

The stress components needed to compute f in each path are obtained from the strain components using the elastic-plastic constitutive relations, in our case the well-known Ramberg-Osgood relation, shown in Equation 18, is used.

$$\frac{\varepsilon_e}{\varepsilon_0} = \frac{\sigma_e}{\sigma_0} + \alpha\left(\frac{\sigma_e}{\sigma_0}\right)^n \tag{18}$$

where σ_e and ε_e are the equivalent stress and strain, σ_0 and ε_0 $(= \sigma_0/E)$ are the yield stress and strain, n, α and E the hardening exponent, the material constant, and the elastic modulus, respectively. The equivalent Von Mises strain shown in Equation 19. The strain along the z-direction can be computed according to Hooke's law in the case of plain stress from the x and y components as: $\varepsilon_z = \frac{-\nu}{(1-\nu)}\left(\varepsilon_x + \varepsilon_y\right)$.

The tangential stresses are null on the plane, and therefore ε_{xz} and ε_{yz} are null.

$$\varepsilon_e = \frac{2}{3}\sqrt{\varepsilon_x{}^2 + \varepsilon_y{}^2 + \varepsilon_z{}^2 - \varepsilon_x\varepsilon_y - \varepsilon_x\varepsilon_z - \varepsilon_y\varepsilon_z + 3\varepsilon_{xy}{}^2} \tag{19}$$

The Ramberg-Osgood parameters α, n and σ_0 are be obtained by an experimental characterization of the material.

Following the approach used in [17], the constitutive relation can be written as shown in Equation 20.

$$\varepsilon_{ij} = \frac{1+\nu}{E}s_{ij} + \frac{1-2\nu}{3E}\sigma_{kk}\delta_{ij} + \frac{3}{2}\alpha\varepsilon_0\left(\frac{\sigma_e}{\sigma_0}\right)^{n-1}\frac{s_{ij}}{\sigma_0} \tag{20}$$

where ν, δ_{ij} and s_{ij} are the Poisson's ratio, Kronecker delta and the stress deviator, respectively. The stress deviator is defined as shown in Equation 21:

$$s_{ij} = \sigma_{ij} - \frac{\sigma_{kk}}{3}\delta_{ij} \tag{21}$$

The strain energy density W can be computed, following Anderson [31], as shown in Equation 22.

$$W = \frac{1}{E}\left[\frac{1}{2}\sigma_e{}^2 + \frac{1}{2}(1-2\nu)\left(\sigma_x\sigma_y - \tau_{xy}{}^2\right) + \frac{\alpha n}{n+1}\sigma_e{}^2\left(\frac{\sigma_e}{\sigma_0}\right)^{n-1}\right] \tag{22}$$

3. Results

In this section some of the results of [21] and [22] are reported for sake of comparison of the two different DIC-based methodologies, the complete set of experimental data can be retrieved from the aforementioned papers.

3.1 Stress intensity factors by the DIC displacement field interpolation

In figure 5, the v components of the displacement as measured by DIC are reported for the Mode Mixity from pure Mode I to roughly 50%, while in figure 6 both the u and v displacements are shown in the case of nearly pure Mode II.
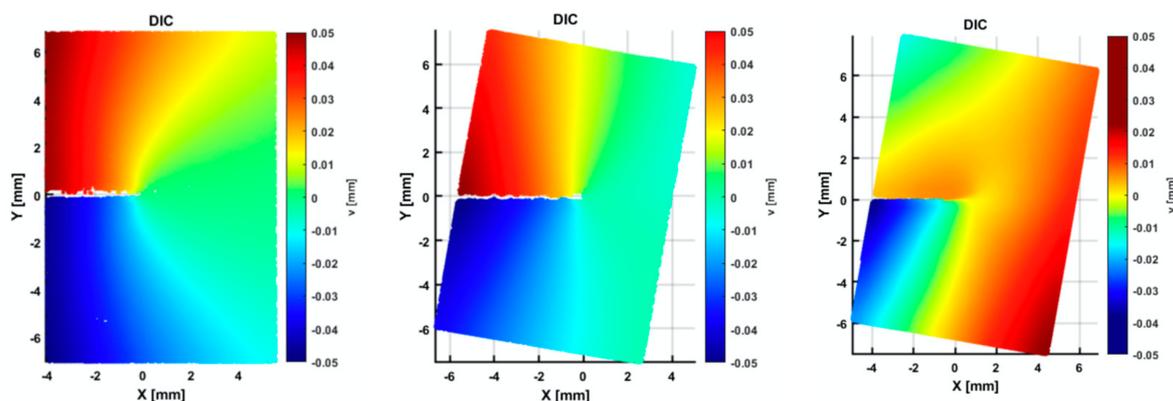

Figure 4: Measurement of the *v* displacement by DIC for Mode Mixity values $(1, 0.77, 0.48)$
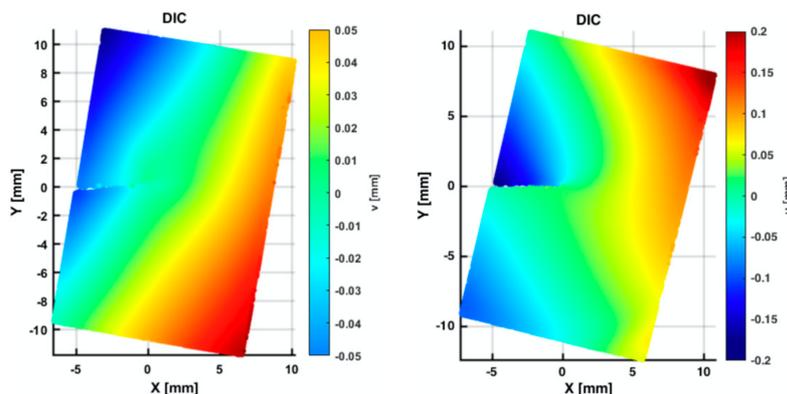

Figure 5: Measurement of the *v* and *u* displacement by DIC for Mode Mixity 0.12

The values of Stress Intensity Factors calculated according to the Equations 7 and 8 can be compared to those obtained from the Load-Displacement curve and the geometry factors defined for the IASCB specimens (PCR henceforth) as shown in Equations 23-24 (where *P* is the critical load, *a* is the crack length, *R* and *t* are the specimen radius and thickness and Y_I and Y_{II} are geometry factors calculated by FEM for the specific geometry [33].

$$K_I = \frac{P}{2Rt}\sqrt{\pi a Y_I} \tag{23}$$

$$K_{II} = \frac{P}{2Rt}\sqrt{\pi a Y_{II}} \tag{24}$$

In figure 6, the values of the SIFs obtained by the DIC procedure, and by the PCR method are compared for different values of Mode Mixity. A good agreement can be seen for Mode II while a large discrepancy is found for Mode I, in particular when it is pure.
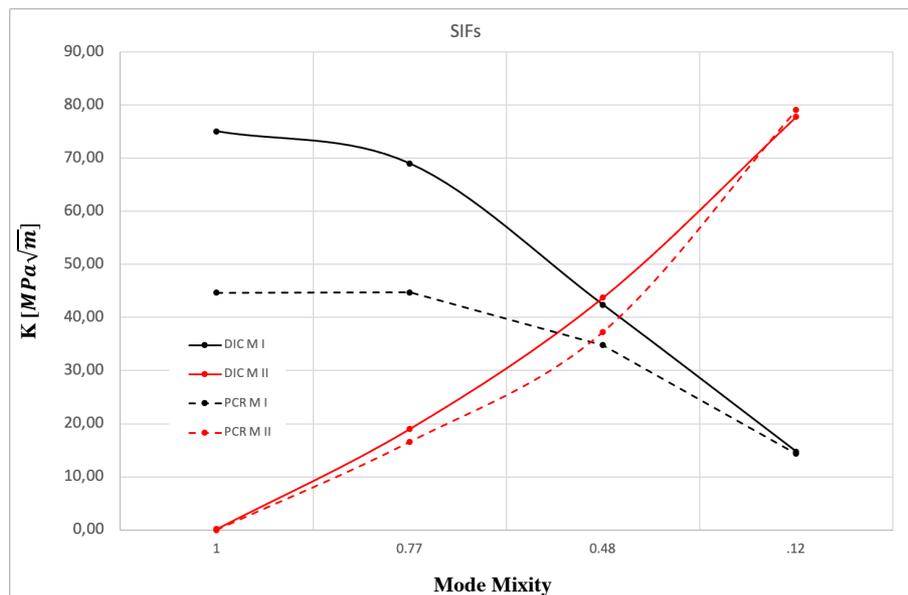
Figure 6: SIFs as a function of the mode mixity: comparison between DIC and PCR

This discrepancy cannot be provoked by the small plastic zone at the crack-tip, which by elementary fracture mechanics, could be responsible for not more than 5% of the difference. On the other side, it is well known, see Anderson, page 76 [31] that the K_I depends on the three-dimensional stress state at the crack tip. More specifically, it is higher for thin specimens, which are in-plane stress condition, while it decreases monotonically as specimen thickness increase until a plane-strain state is reached, and the outermost layers of materials become less important in the overall behavior.

In our case, the overestimation of the K_I obtained by DIC based technique is because the methodology evaluates the SIF from the displacement field measured on the outer surface, which is in-plane stress condition. This phenomenon becomes less important reducing the Mode Mixity until Mode II is reached.

3.2 . J-integral computed utilizing DIC

The J-integral was computed on different rectangular domains, similar to the one shown in figure 3, having removed the data within 0.3 mm (this value was determined empirically) from the crack axis because particularly noisy, due to the massive plasticization and to the crack opening. The value of the J-Integral was obtained by averaging on these paths a few millimeters long since, due to the data discretization, the integral was not strictly path-independent.

Figure 7 shows, as examples, the x and y displacement and strain maps obtained by the DIC two extreme configurations tested, pure Mode I and nearly pure Mode II. It can be observed that the strain in y and in the x-direction (in particular) increases going from Mode I to Mode II, which lead to a higher strain energy work to make the crack propagate.
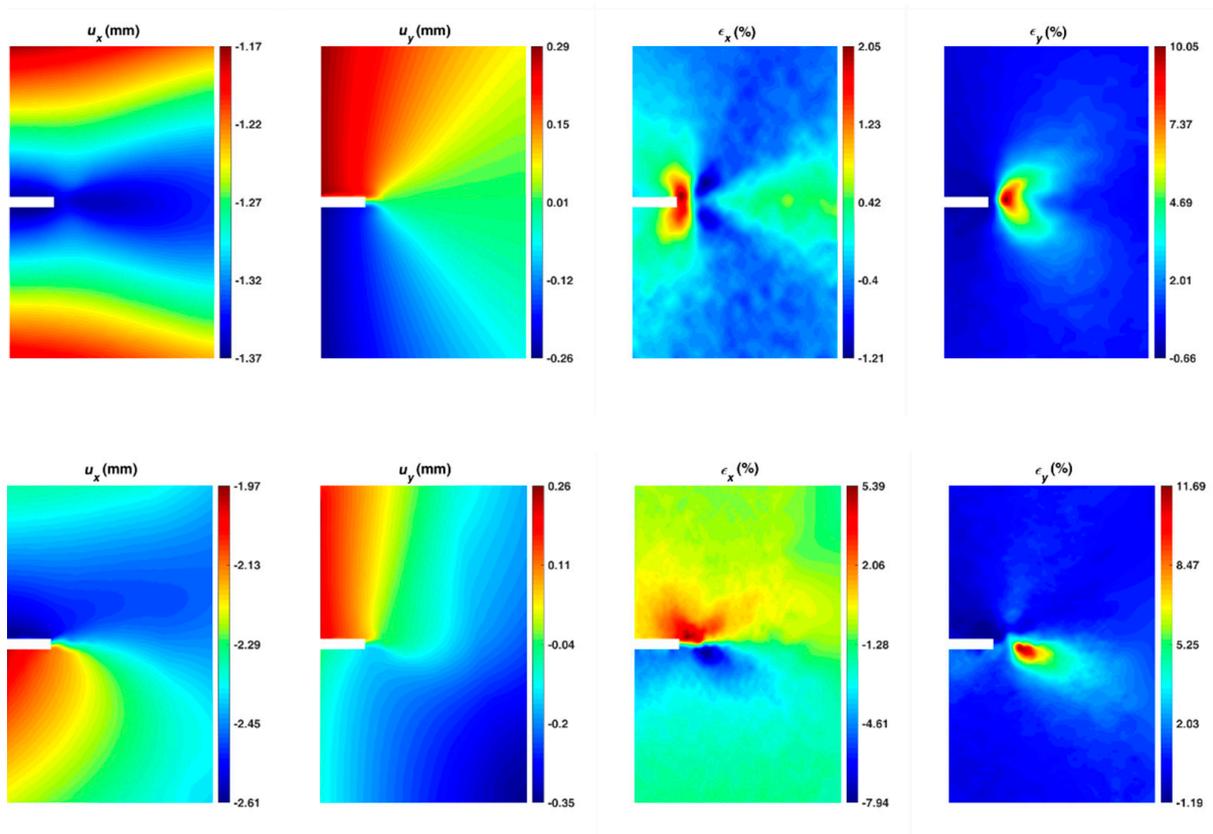
Figure 7: Measurement displacement and strain DIC for Mode Mixity values 1 and 0.12

As shown in [22] the J-integral can be derived by the Load-Displacement curve (LDC Method) once the indentation due to the support pressure has been removed and geometry factors dependent on the specimen shape and loading conditions are applied. In figure 8, the J-integral values computed through both methods are shown.
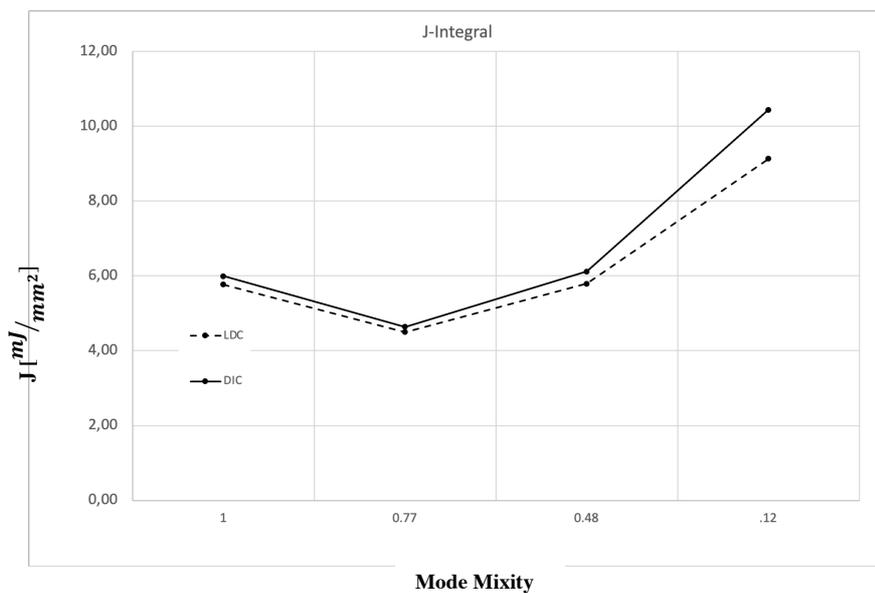

Figure 8: J-Integral versus the Mode Mixity as calculated by the DIC and LDC methodologies

Like in the previous case the DIC based technique tends to slightly overestimate the fracture mechanics parameter, but for all the Mode Mixity values. The J-integral is significantly higher in Mode II as it is well-known in literature [22].

4. Discussion

The two methods based on DIC which were shown, have some unique capabilities, but also some limitations to be considered. As recalled already in the title, by AM it is possible to produce crack-like notches, but not real cracks. The minimum radius of curvature depends on the technology and in the cases reported it was around 90 micrometers. The possibility to make this crack grow by fatigue pre-cracking is linked to the component geometry and loading. Moreover, it would be tricky to make the crack propagate exactly in the desired direction. References [21, 22] show the difference with respect to an actual crack in Mode I, which is more marked in the case of materials having higher-yielding strength.

On the other side, the possibility to embed crack-like notches of any shape, in any position and with any orientation in a model of a component can provide new design tools or validation benchmarks for numerical models. In the case of thick components, the evaluation of the fracture parameters by DIC on the surface can lead to an overestimation of the SIFs for high values of Mode Mixity, near to pure Mode I. To overcome this problem, a full 3D numerical analysis should support the DIC measurements (in general this task is quite straightforward since a detailed 3D model is necessary for the AM phase).

A very promising approach is the one based on the evaluation of the J-integral, which provides results very similar to the ones obtained by LDC in the case of specimens, where both are applicable.

The general limitation of these methods is the need to capture by two cameras in the most general 3D case the image of a surface in the immediate vicinity of the crack-dominated zone.

The methodologies described can be used also in the case of non-artificial cracks, with the same limitations above listed.

5. Conclusion

Two methodologies based on DIC have been shown in detail and compared in the case of IASCB specimens containing additive manufacture crack-like notches.
The main findings are:
- by DIC measurement of the displacement it is possible to evaluate the SIFs using the interpolation of the William's model.
- by DIC measurement of the displacement and by the derivation of the strain and stresses (using a material constitutive equation) it is possible to evaluate the average J-integral around the crack tip.
- The values obtained by the first method are overestimated in the case of pure Mode 1 with respect to the results obtained from the load-displacement curve.
- The values obtained by the second method are in good agreement with the results obtained from the load-displacement curve.

6. References

[1]   Reza Khosravani M., Berto F-, Ayatollahi M.R., Reinicke T., 2020, Fracture behavior of additively manufactured components: A review, *Theor. Appl. Fract. Mech.* 109, 102763
[2]   Brugo, T.; Palazzetti, R.; Ciric-Kostic, S.; Yan, X. T.; Minak, G.; Zucchelli, A., 2016, Fracture Mechanics of Laser Sintered Cracked Polyamide for a New Method to Induce Cracks by Additive Manufacturing. *Polym. Test.* **50**, 301–308.
[3]   Peters, W. H., Ranson, W. F., Kalthoff, J. F., & Winkler, S. R., 1985,. A study of dynamic near-crack-tip fracture parameters by digital image analys. *J. Phys. Colloq*, **46** (C5), C5–631–C5–638.
[4]   McNeill, S.R., Peters, W.H., Sutton, M.A., 1987, Estimation of stress intensity factor by digital image correlation. *Eng Fract Mech*, **28** (1), 101-112.
[5]   Peters, W. H. and Ranson, W. F., 1982, Digital imaging techniques in experimental stress

analysis. *Opt Eng,* **21** (3), 427-431.

[6]   Sutton, M.A., Wolters, W.J., Peters, W.H., Ranson, W.F., McNeill, S.R., 1983, Determination of displacements using an improved digital correlation method. *Image Vision Comput.* **1**, 133–139.

[7]   Gubeljak, N., Semenski, D., Drvar, N., Predan, J., Kozak, D., Oblak, M., 2006, Object grating method application in strain determination on ctod tests // *Strain*, **42** (2) 81-87.

[8]   Muskhelishvili, N.I., 1977, *Some basic problems of the mathematical theory of elasticity*, 4th edition, Noordhoff International, Leyden, The Netherlands

[9]   Nurse, A. D., Patterson, E. A.,1993, Determination of Predominantly Mode II Stress Intensity Factors from Isochromatic Data. *Fat Frac Eng Mat Struct* **16** (12), 1339–1354.

[10]   Lopez-Crespo, P., Shterenlikht, A., Patterson, E. A., Yates, J. R., Withers, P. J., 2008, The Stress Intensity of Mixed Mode Cracks Determined by Digital Image Correlation. *J Strain Anal Eng* **43** (8), 769–780.

[11]   Williams, J.G., Ewing, P.D., 1972, Fracture under complex stress – the angled crack problem. *Int J Fracture*, **8**:441–6.

[12]   Papadopoulos, G. A., Poniridis, P. I., 1989, Crack Initiation under Biaxial Loading with Higher-Order Approximation. *Eng. Fract. Mech.*, **32** (3), 351–360.

[13]   Silva, A. L. L., de Jesus, A. M. P., Xavier, J., Correia, J. A. F. O., 2017, Fernandes, A. A. Combined Analytical-Numerical Methodologies for the Evaluation of Mixed-Mode (I + II) Fatigue Crack Growth Rates in Structural Steels. *Eng. Fract. Mech*, **185**, 124–138.

[14]   Rice, J.R., 1968, A path independent integral and the approximate analysis of strain concentration by notches and cracks. *J. Appl. Mech. ,* **35**, 379–386.

[15]   Vavrik, D., Jandejsek, I., 2014, Experimental Evaluation of Contour J Integral and Energy Dissipated in the Fracture Process Zone. *Eng. Fract. Mech.*, **129**, 14–25

[16]   Kozłowiec, B. , 2017, Numerical Methods for Estimating J Integral in Models with Regular Rectangular Meshes. *Iop. Conf. Ser. Mater. Sci. Eng.* **175**, 012062,

[17]   Breitbarth, E., Strohmann, T., Besel, M., Reh, S., 2019, Determination of Stress Intensity Factors and J Integral Based on Digital Image Correlation. *Frat. ed Integrita Strutt.*, **13**, 12–25.

[18]   Catalanotti, G.,2010, Measurement of Resistance Curves in the Longitudinal Failure of Composites Using Digital Image Correlation. *Compos. Sci. Technol.*, **70**, 1986–1993.

[19]   Shih, C.F., Moran, B., Nakamura, T., 1986, Energy Release Rate along a Three-Dimensional Crack Front in a Thermally Stressed Body. *Int. J. Fract.* **30**, 79–102.

[20]   Gonzáles, G.L.G., González, J.A.O., Castro, J.T.P., Freire, J.L.F., 2017, A J-Integral Approach Using Digital Image Correlation for Evaluating Stress Intensity Factors in Fatigue Cracks with Closure Effects. *Theor. Appl. Fract. Mech.* **90,** 14–21.

[21]   Campione, I., Brugo, T.M., Minak, G., Tomić, J.J., Bogojević, N., Kostić, S.Ć., 2020, Investigation by Digital Image Correlation of Mixed Mode I and II Fracture Behavior of Metallic IASCB Specimens with Additive Manufactured Crack-Like Notch. *Metals* **10**, 400.

[22]   Brugo, T.M., Campione, I., Minak, G. ,2021, Investigation by Digital Image Correlation of Mixed-Mode I and II Fracture Behavior of Polymeric IASCB Specimens with Additive Manufactured Crack-Like Notch. *Materials* , *14*, 1084.

[23]   Saghafi, H., Monemian, S., 2010, A New Fracture Toughness Test Covering Mixed-Mode Conditions and Positive and Negative T-Stresses. *Int J Fract* , **165** (1), 135–138.

[24]   Ayatollahi, M. R., Aliha, M. R. M.;,Saghafi, H. 2011, An Improved Semi-Circular Bend Specimen for Investigating Mixed Mode Brittle Fracture. *Eng. Fract. Mech.*, **78** (1), 110–123.

[25]   Saghafi, H., Zucchelli, A., Minak, G., 2013, Evaluating Fracture Behavior of Brittle Polymeric Materials Using an IASCB Specimen. *Polymer Testing*, **32** (1), 133–140.

[26]   Palanca, M., Brugo, T. M., Cristofolini, L., 2015, Use of Digital Image Correlation to Investigate the Biomechanics of the Vertebra. *J. Mech. Med. Biol.* **15** (02), 1540004.

[27]   Williams, M. L., 1957, On the Stress Distribution at the Base of a Stationary Crack. *J Appl Mech*

, **24** (6), 109-114.

[28]   Yates, J. R., Zanganeh, M., Asquith, D., Tai, Y. H., 2010, Quantifying Crack Tip Displacement Fields: T-Stress and CTOA. *Eng. Fract. Mech.*, **77** 2063–2076

[29]   Yoneyama, S., Ogawa, T., Kobayashi, Y., 2007, Evaluating Mixed-Mode Stress Intensity Factors from Full-Field Displacement Fields Obtained by Optical Methods. *Eng. Fract. Mech.*, **74** (9), 1399–1412.

[30]   Yamane, H.,Arikawa, S., Yoneyama, S.; Watanabe, Y., Asai, T., Shiokawa, K., Yamashita, M., 2014, J-Integral Evaluation for an Interface crack using digital image correlation, *J. of JSEM*, **14**, 122-127.

[31]   Anderson, T.L. ,2017, *Fracture Mechanics: Fundamentals and Applications*; CRC Press: Boca Raton, FL, USA

[32]   Darban, H. Haghpanahi, M. Assadi, A. , 2011, Determination of crack tip parameters for ascb specimen under mixed mode loading using finite element method. *Comput. Mater. Sci.*, **50,** 1667–1674.

Acknowledgments